INTERFACE

royalsocietypublishing.org/journal/rsif

CC BY

Research

**Cite this article:** Bano S, Bibi T, Khan MI, Shah KU, Ud-din F, Ali H, Shehzad A, Seo EK, Khan S. 2026 Band gap energy shift as a biophysical marker of Puerarin's neuroprotective role in epilepsy-induced demyelination. *J. R. Soc. Interface* **23**: 20250990.
https://doi.org/10.1098/rsif.2025.0990

Received: 25 September 2025
Accepted: 10 February 2026

**Subject Category:**
Life Sciences–Chemistry interface

**Subject Areas:**
biochemistry, bioinformatics, chemical biology

**Keywords:**
epilepsy, neuropharmacology, neuroscience

**Author for correspondence:**
Salman Khan
e-mail: skhan@qau.edu.pk

Electronic supplementary material is available online at https://doi.org/10.6084/m9.figshare.c.8329018.

THE ROYAL SOCIETY PUBLISHING

# Band gap energy shift as a biophysical marker of Puerarin's neuroprotective role in epilepsy-induced demyelination

Shahar Bano[1], Tehmeena Bibi[2], Muhammad Ibrar Khan[1,3], Kifayat Ullah Shah[2], Fakhar Ud-din[2], Hussain Ali[2], Adeeb Shehzad[4], Eun Kyoung Seo[5] and Salman Khan[1]

[1]Department of Pharmacy, Quaid-i-Azam University, Faculty of Biological Sciences, Islamabad, Islamabad Capital Territory, Pakistan
[2]Department of Pharmacy, Quaid-i-Azam University, Islamabad, Islamabad Capital Territory, Pakistan
[3]Department of Pharmacy, Capital University of Science and Technology, Islamabad, Islamabad Capital Territory, Pakistan
[4]Research Center, Dhofar University, Salalah 211, Oman
[5]College of Pharmacy, Ewha Womans University, Seoul 03760, South Korea

SB, 0009-0003-7141-1974; MIK, 0009-0003-8312-2520; FU, 0000-0001-9537-4897; SK, 0000-0002-6226-8470

The study aims to determine the neuroprotective effect of Puerarin, extracted from *Pueraria lobata* roots, against pentylenetetrazole (PTZ)-induced epileptic seizures and concomitant demyelination and low conductance through diffuse reflectance spectroscopic (DRS) technique. Mice groups ($n$ = 12) were pretreated with vehicle and Puerarin (100 mg kg$^{-1}$, intraperitoneal (i.p.)) for 42 days (alternate days). PTZ (35 mg kg$^{-1}$, i.p.) was given after 30 min to all mice groups except the vehicle control group. Puerarin remarkably reduced seizures scoring, hyperalgesia and blood-brain barrier disruption and improved muscle coordination. High anti-myelin oligodendrocyte glycoprotein (anti-MOG) levels in PTZ-treated mice confirmed demyelination, with low molar absorption coefficient ($\mu_a$) and high scattering coefficient ($\mu_s$) and absorption. Puerarin treatment increased $\mu_a$ and decreased anti-MOG and $\mu_s$, similar to the vehicle control group. This indicates a protective effect of Puerarin against demyelination. Band gap energy ($E_{bg}$) was calculated by the Kubelka–Munk model and incorporated in the current study for the first time to evaluate pathology. $E_{bg}$ blue shift showed compromised conductance capacity of nerves in PTZ-induced epilepsy compared with Puerarin-treated animals. Haematoxylin and eosin and Nissl staining were used to further authenticate the neuroprotective effect of Puerarin. In conclusion, Puerarin countered demyelination and low conductance of nerve owing to PTZ-induced epilepsy assessed via DRS.

## 1. Introduction

Epilepsy is a neurological disorder that is common among 50 million population and causes lifetime suffering in 10% of epileptic patients [1]. Hyperstimulation of neuronal electrical activity leads to recurring seizures [2]. Chronic agitated neuronal activity causes a disparity in neurotransmitters that control excitation and inhibition, affecting the neuronal network and resulting in neuronal loss [3,4]. Subsequently, blood-brain barrier (BBB) disruption and the intrusion of leukocytes occur, leading to immune system activation [5,6]. As a result, autoantibodies are formed against myelin oligodendrocyte glycoprotein (MOG), which is produced by oligodendrocytes in the central

© 2026 The Authors. Published by the Royal Society under the terms of the Creative Commons Attribution License http://creativecommons.org/licenses/by/4.0/, which permits unrestricted use, provided the original author and source are credited.

Downloaded from royalsocietypublishing.org/rsif/article-pdf/doi/10.1098/rsif.2025.0990/6127383/rsif.2025.0990.pdf
by guest
on 22 September 2026

nervous system (CNS) [7]. Myelination aids in conduction and communication among the nerves [8]. Therefore, several studies reported CNS demyelination and low conductance in epilepsy [9]. However, the anti-seizures medication (ASM) is designed only to manage symptoms, and concomitant pathologies are less considered in ASM research [10].

Concomitant pathologies diagnosis is challenging in clinical practice, and it includes various examination and assessment techniques [11,12]. Hence, demyelination and low conductance in epileptic patients remain a matter of concern. The pentylenetetrazole (PTZ)-induced chronic epileptic seizures model was used in the study as it is illustrative of human epileptic seizures [13]. Diffuse reflectance spectroscopy (DRS) and the Kubelka–Munk model are already in use for research on neurological disorders [14]. Absorption and scattering coefficients indicate the extent of demyelination [15]. However, the concept of band gap energy was corroborated in a study to detect changes in conductance [16]. DRS was used, and the Kubelka–Munk model was applied for band gap energy calculation [17]. Conductors have 0 eV, while insulators have a higher (greater than 15 eV) band gap energy [18]. Similarly, in the brain, myelinated nerves conduct impulses through ion flow via channels, demonstrating conductance [19]. Thus, the concept was used to evaluate the conductance ability of brain samples. The process was easier to perform, and the results are relatively less affected by human error than conventional methods that need more professional training and handling practice.

Natural compounds are gaining more attention in the treatment of ailments owing to their fewer side effects [20]. Puerarin, an isoflavone, is extracted from the roots of the kudzu plant, scientifically known as *Pueraria lobata*, and is commonly used in Chinese medicine [21]. Puerarin is reported to possess anti-diabetic, anti-oxidant, anti-inflammatory, anti-tumour, anti-apoptotic, hepatoprotective and neuroprotective properties [22–24]. The bioactive compound is gaining attention from scientists owing to its high efficacy and fewer adverse effects [25]. However, the Puerarin effect in demyelination and low conductance has not been studied specifically in epilepsy. Therefore, the effect of Puerarin was evaluated in demyelination and low conductance caused by chronic epilepsy. The spectroscopic results were compared and authenticated by using conventional methods of haematoxylin and eosin (H&E) staining and enzyme-linked immunosorbent assay (ELISA) in order to confirm the pathological changes.

# 2. Material and methods

## 2.1. Chemicals and materials

Puerarin was provided by Prof. Eun Kyoug Seo, College of Pharmacy, Graduate School of Pharmaceutical Sciences, Seoul, South Korea. Dimethyl sulfoxide (DMSO), 0.9% saline solution, Evans blue dye, formalin, haematoxylin dye, eosin dye and paraformaldehyde were purchased from Sigma-Aldrich, USA. Elisa kit (lot number F240319AD) for anti-MOG was purchased from Euroimmun, Germany. Analytical grade chemicals were used in the study.

## 2.2. Animals and ethical approval

Current research work was performed on male albino mice (BALB/c) of weight 25–30 g obtained from the National Institute of Health (NIH), Islamabad, Pakistan. The experiment was performed as per the guidelines of NIH. A stress-free living environment was provided to animals with sufficient supply of food and water. The study was held after attaining ethical approval (BEC-FBS-QAU2022-422) of the Bioethical Committee, Quaid-i-Azam University, Islamabad, and compliance was ensured as per guidelines. All animals were acclimatized for a week in the laboratory conditions and divided into three groups having 12 animals in each group considering the mortality rate. Baseline values of weight were noted and documented.

## 2.3. Pentylenetetrazole-induced chronic epilepsy model

Epilepsy was induced using PTZ in mice groups ($n$ = 12) by following set protocols with minor modifications, keeping in view the prognosis of demyelination [6,26,27]. The schematic diagram representing the complete study design with time intervals has been demonstrated in figure 1. In brief, the complete period of the chronic model was 42 days, while induction and treatment were performed on alternate days. Animals were divided into three groups with administration of vehicle control, Puerarin (100 mg $kg^{-1}$) and PTZ (35 mg $kg^{-1}$) as follows:

*Group I*. Vehicle control group received only vehicle (DMSO 2% and normal saline).

*Group II*. PTZ administered group received only 35 mg $kg^{-1}$ PTZ i.p. injection, and subject to 30 min of observations for seizure scoring.

*Group III*. Animals pretreated with Puerarin (100 mg $kg^{-1}$). After 30 min, PTZ (35 mg $kg^{-1}$) i.p. injection was given and the animals were monitored for 30 min for seizure scoring.

Epileptic seizures were analysed according to Racine's scale [28,29]. On day 42, animals were dissected, and sampling was done.

## 2.4. Kondziela's inverted screen test to assess muscle coordination

Demyelination of the nerves and reduced conductivity compromise muscle coordination [30]. Therefore, Kondziela's inverted screen test was performed in order to assess the effect of Puerarin on PTZ-induced epileptic seizures in mice. Set protocols were

Downloaded from royalsocietypublishing.org/rsif/article-pdf/doi/10.1098/rsif.2025.0990/6127383/rsif.2025.0990.pdf
by guest
on 22 September 2026

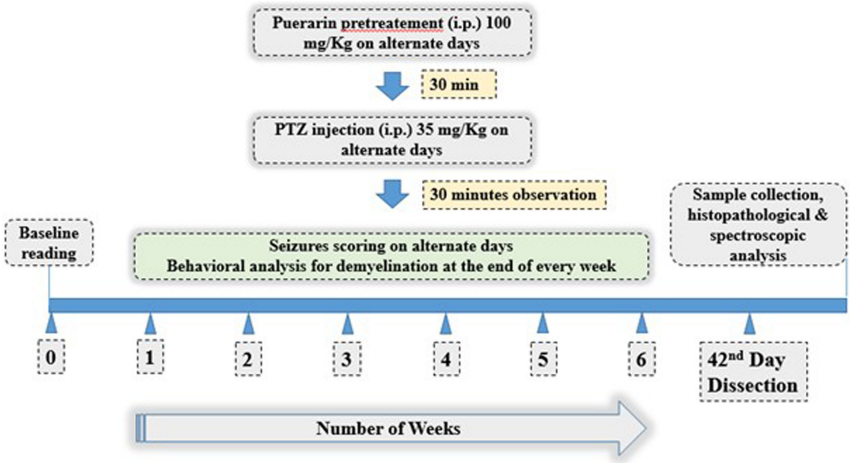



**Figure 1.** Study design of demyelination and reduced nerve conductivity induced by PTZ-induced epileptic seizures in mice.

followed to assess the motor coordination [31,32]. In brief, baseline readings were recorded by placing mice in the centre of a mesh screen without administering any drug. The mesh was inverted, and animals were observed for the next 60 s to fall on a cushioned surface. The time for fall was recorded and noted as the cut-off time. Similarly, readings were taken and noted for vehicle control, epileptic and treatment groups. Behavioural assessment was performed at the end of every week after the last injection of PTZ in order to determine the demyelination development.

## 2.5. Hot plate method for thermal hyperalgesia

Nerve demyelination and low conductivity can be a possible cause of hyperalgesic response to external thermal stimuli in epilepsy [33]. The hot plate method was used to detect the change in the perception of heat stimuli at the end of every week after the last injection of PTZ. The experiment was performed by exposing the mouse to the preheated hot plate at 55°C. The mouse was observed for the cut-off time of 35 s. Time noted for withdrawal or licking of hind paw. The experiment was performed at the end of every week during the 42 day chronic epilepsy model.

## 2.6. Evans blue test for assessment of blood-brain barrier dysfunction

Owing to the chronic hyperexcitation of neurons, the BBB becomes compromised, leading to the invasion of immune cells [34]. Resultantly, activation of the immune system and formation of autoantibodies occur against the myelin sheath of CNS neurons [35]. The permeability for immune cells was assessed by applying the Evans blue (EB) test as per established protocols [36]. The experiment was performed on the 42nd day of the chronic epilepsy model. Three animals from each group were taken and administered with 2% of EB dye (2 ml $kg^{-1}$) in the tail vein. Subsequently, perfusion with saline injection was done after 30 min. Animals were dissected, and extracted brains were homogenized after adding phosphate buffer and trichloroacetic acid, each 2.5 ml. The homogenate was subject to 30 min of centrifugation (1000*g*), and the supernatant was separated. A microplate reader was used to determine optical density at 620 nm. EB concentration (µg) per gram of brain tissue was reported in the results [37].

## 2.7. Enzyme-linked immunosorbent assay for the detection of anti-myelin oligodendrocyte glycoprotein antibodies

MOG is essential for the myelination of nerves as well as for communication between cells [38,39]. BBB disruption and immune cell infiltration cause the production of antibodies against MOG that potentiate demyelination [40]. ELISA (Euroimmun, Germany, containing lot number F240319AD Exp. date: 18-09-2025) was performed to detect if immuno-reactivity was the possible reason for demyelination and low nerve conductance or not. Briefly, samples were taken as brain tissue extract prepared from brain tissue homogenate (200 mg tissue in 1 ml of cell extraction buffer). Samples, standards and reagents were prepared as per the instructions provided with the kit. Samples and standards, 50 µl each, were loaded in the wells. Antibody solution (50 µl) was added to all wells of the samples and standard and incubated for 1 h at room temperature. Each well was aspirated and washed with wash buffer three times. A development solution of 100 µl was added to all wells and again incubated for 10 min. After incubation, a stop solution of 100 µl was added to each well, and then the optical density (OD) was checked at 450 nm wavelength. Analysis was performed in triplicate and results demonstrated in percentage (%).

## 2.8. Diffuse reflectance spectroscopy

The technique is already in use for the detection of neurological disorders. Optical properties of tissue samples vary in disease conditions; therefore, these techniques are of great significance in pathological condition diagnosis [14]. Moreover, researchers have been using this technique in the development of new treatments [41,42]. DRS was performed by adopting the reported methodology with some modifications. The aim was to use the intact brain samples without any chemical processing and

Downloaded from royalsocietypublishing.org/rsif/article-pdf/doi/10.1098/rsif.2025.0990/6127383/rsif.2025.0990.pdf
by guest
on 22 September 2026

sampling techniques to get results without any extra peaks of solutions or buffers. Sample preparation was performed in controlled temperature surroundings. Pre-autoclaved glass slides (0.8 mm) were taken and cleaned with ethanol to avoid any contamination. On the last day of the chronic epilepsy model, animals were dissected, and brains from each group were extracted. Freshly extracted brains ($n$ = 3) from each group were frozen at −20°C for 24 h. At low temperature, frozen samples were mounted on cleaned glass slides previously placed on ice packs. Instantly, samples were covered with cling film for protection. Cling film was used because it has no distortion characteristics in the spectra of samples [43]. The empty clean slides were covered with a cling sheet and scanned on a LAMBDA 950 UV/Vis/NIR Spectrophotometer by PerkinElmer Inc. The screening was performed for zero correction to avoid any interfering peaks in the results. After that, glass slides mounted with brains were scanned one by one for the complete wavelength (200–1200 nm) of the instrument. UV WinLab Data Processor and Viewer by Perkin was used for obtaining spectra of each sample.

## 2.9. Data processing and analysis

Reflection calibration was performed by using barium sulfate as a reflection standard. Baseline correction and auto-calibration of the instrument were done. To remove the interference of other factors, an empty, clean glass slide was covered with a cling sheet and screened for the full wavelength to subtract from the samples. After completing the scanning of empty glass slides, the auto-calibration of the instrument was done. The data were extracted in the form of per cent transmittance ($\%T$) spectra. The instrument provides results with accuracy and precision of less than or equal to 0.0007%$T$ with less than or equal to 0.005 nm wavelength resolution. All samples, prepared as described above, were loaded on the instrument one by one and scanned for extraction of transmittance spectra. Optical densities (absorbance) of samples were calculated using the Beer–Lambert Law equation from per cent transmittance [44],

$$\text{Absorbance} = A = 2 - log(\%T)\,.$$

Reflectance ($R$) of the samples was calculated from absorbance and transmittance [45]. The following equation was used for the calculation of reflectance:

$$\text{Absorbance} = 100 - (\text{Reflectance} + \text{Transmittance}) = 100 - \text{Reflectance} - \text{Transmittance}$$

by rearranging the equation

$$\text{Reflectance} = 100 - \text{Absorbance} - \text{Transmittance} = 100 - (\text{Absorbance} + \text{Transmittance}),$$

hence, taking reflectance as

$$R = 100 - (A + T),$$

calculation provided with reflectance and absorbance parameters of brain samples. The data were further processed to get the ratio of molar absorption coefficient ($\mu_a$) and reduced scattering coefficient ($\mu_s$).

Here,

$$Molar\ absorption\ coefficient = \mu_a = (1 - R)^2,$$

while

$$Reduced\ scattering\ coefficient = \mu_s = 2R\,.$$

The ratio was estimated by using Kubelka–Munk theory, assuming the brains as samples with infinite thickness and a black background [46–48]. The Kubelka–Munk model was simulated as it is simple to apply and suitable for chemical and structural complexity. Therefore, the following equation was considered for obtaining the molar absorption coefficient and scattering coefficient ratio [49,50]:

$$F(R_\infty) = \frac{\mu_a}{\mu_s} = \frac{K}{S} = \frac{(1 - R)^2}{(2R)},$$

where $F(R_\infty)$ is the Kubelka–Munk Function, ∞ the sign represents the thickness of the sample, $K$ is the molar absorption coefficient ($\mu_a$) that is a distinct intrinsic property of brain tissues to absorb the energy in the form of photons. However, $S$ denotes the reduced scattering coefficient ($\mu_s$) of brain tissues that represent the light multiple scatterings incidents when striking the tissue owing to the presence of various light scatterers.

To find the band gap energy shift ($E_{bg}$), $F(R_\infty)*h\nu^{1/2}$ was plotted against the energy of the photon. The energy of the photon was taken by using Max Planck's equation as under

$$E = h\nu = \frac{hc}{\lambda},$$

where $E$ represents the energy of the photon, $h$ represents Planck's constant, ν represents the frequency of a light wave, $c$ denotes the speed of light and $\lambda$ shows the wavelength. Hence, direct $E_{bg}$ was calculated by plotting $(F(R_\infty)*h\nu)^{1/2}$ against $h\nu$ in electron volts (eV) [19,50].

Downloaded from royalsocietypublishing.org/rsif/article-pdf/doi/10.1098/rsif.2025.0990/6127383/rsif.2025.0990.pdf
by guest
on 22 September 2026

## 2.10. Estimation of nerve conductance through band gap energy

The concept of band gap energy refers to the difference in energies between valence band ($E_V$) and the conductance band ($E_C$) of the material [16]. The lower energy difference denotes that the electrons get excited and move to the conduction band for the electrical conductivity [51]. Therefore, the lower band gap energy of brain samples shows a higher ability of the sample to conduct electrical signals, and a higher energy difference is related to lower conductance ability. Usually, band gap energy in the range of 0.1–6 eV shows semiconductor behaviour of the samples. Conductors have an energy gap below this energy range; however, insulators show band gap energy of more than 6 eV [52]. Based on the description above, the relationship between intrinsic electrical conductivity ($\sigma$) and band gap energy can be expressed as follows:

$$Electrical\ conductivity\ (\sigma) = \frac{1}{Band\ gap\ energy} = \frac{1}{E_{bg}}.$$

Hence, if band gap energy reduces, nerve conductance enhances owing to potential intact ions flow having valence and conductance bands across the nerves and synaptic cleft for transmission of impulse. However, the damaged and demyelinated nerves owing to immuno-reactivity caused by epilepsy will have comparatively less impulse generation and transmission ability.

## 2.11. Histopathological examination of brain regions using haematoxylin and eosin staining

Phosphate buffer saline (PBS) and 4% paraformaldehyde were used for perfusion of anaesthetized animals. Immediately after the perfusion, brains ($n$ = 3) of animals were extracted subsequent to dissection. Tissues were sectioned using a microtome at a thickness of 4–5 µm at room temperature or 25°C. Tissue sections were again fixed for 12 h in the same fixative at room temperature, i.e. 25°C. Subsequently, tissues were embedded in paraffin wax and finally mounted on glass slides. These slides were used to perform haematoxylin and eosin (H&E) [53]. For histological evaluation and to determine the impact of treatment, three sections of each animal were typically examined using an Olympus microscope from Japan. For quantification, Image J software (NIH, USA) was used.

## 2.12. Nissl staining for histopathological analysis

The structure of neurons in nuclei and layers throughout the nervous system, primarily the brain and spinal cord, is extensively studied using Nissl staining. Three brain samples ($n$ = 3) were taken from each group's animal. Sections of the samples were divided up and fixed in formalin (3%) for 24 h. Each section was further processed, and finally, thin slices of 5 µm were formed from paraffin-embedded blocks. Cresyl violet acetate stain (Thermo Fisher Scientific, Germany) was used for further processing of slide-mounted brain sections as per a previously reported protocol [54–56]. Pyramidal cells that were intact in morphology were counted by observers following blind study protocols. Images were taken and analysed using an Olympus microscope (USA).

## 2.13. Statistical test applied to data

All samples for analysis were taken in triplicate. Therefore, results are reported in mean ± standard deviation (s.d.). For evaluation of behavioural data, GraphPad Prism software was used for the application of statistics and the formation of graphs. Two-way ANOVA was applied to the results of the behavioural evaluation of animals. For diffuse reflectance spectroscopy, Origin software v. 8.5 was used to form graphs and for statistical evaluation.

# 3. Results

## 3.1. Effects on chronic epileptic seizures

Puerarin (100 mg $kg^{-1}$) dose was used as pretreatment for chronic epileptic seizures in the PTZ-induced epileptic seizures model [57]. PTZ-administered mice showed high scoring of epileptic seizures compared with the vehicle control group ($p < 0.001$) during the 42 days of the chronic model. However, Puerarin prominently reduced ($p < 0.001$) the epileptic-seizure scoring compared with the PTZ-administered mice group assessed at the end of every week. The results are presented as mean ± s.d. of the seizure intensity score observed at the end of every week after the last PTZ injection during the whole chronic model of epileptic seizures (figure 2).

## 3.2. Effect on compromised muscle coordination owing to epileptic seizures-led demyelination

Muscle coordination was assessed by observing the latency time to fall every week after 4 h of seizure scoring (figure 3). At the end of the first week of the model, PTZ-administered mice showed compromised muscle coordination at the significance level $p < 0.01$ compared with the vehicle control group. Nevertheless, the significance level was $p < 0.001$ for the remaining weeks.

Downloaded from royalsocietypublishing.org/rsif/article-pdf/doi/10.1098/rsif.2025.0990/6127383/rsif.2025.0990.pdf
by guest
on 22 September 2026

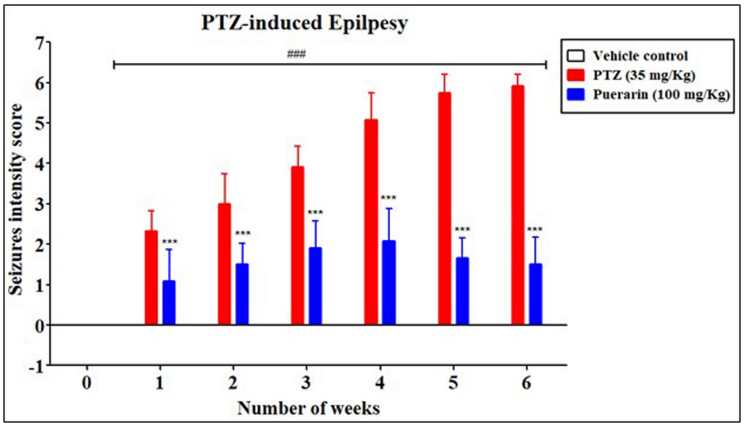



**Figure 2.** Puerarin exhibited a reduction in PTZ-induced epileptic seizures, scoring assessed via Racine's scale. Seizure intensity score is exhibited in mean ± s.d. for 12 mice in each group ($n = 12$). Significance level *** $p < 0.001$ represents comparison of Puerarin effect with PTA-administered group mice; however, ### $p < 0.001$ shows comparison between PTZ-administered mice and vehicle control group of animals.

However, Puerarin (100 mg $kg^{-1}$) considerably improved latency time to fall at a significance level $p < 0.01$ in the first week and $p < 0.001$ on the remaining weeks compared with PTZ-administered mice.

## 3.3. Effect on sensory-motor response owing to demyelination in epileptic seizures

The untreated PTZ-administered group showed thermal hyperalgesia response owing to altered sensory-motor response as a result of epileptic seizures, leading to demyelination. The response ($p < 0.001$) was compared with the vehicle control group. However, Puerarin (100 mg $kg^{-1}$) considerably reduced the thermal hyperalgesia compared with the PTZ-administered group of animals at a significance level $p < 0.001$. Results are presented as mean ± s.d. ($n = 12$) in figure 4.

## 3.4. Effect on blood-brain barrier integrity affected owing to the immune response

The BBB gets compromised in PTZ-induced epileptic seizures, and the effect was visible in PTZ-treated mice when Evans blue dye was administered intravenously. The induction was compared with the vehicle control group. Results showed a high level of Evans blue dye penetration in PTZ-treated mice ($p < 0.001$). Contrary to this, Puerarin (100 mg $kg^{-1}$) prominently ($p < 0.001$) limited the BBB disruption compared with PTZ-treated animals, as shown in figure 5A.

## 3.5. Effect on anti-myelin oligodendrocyte glycoprotein antibody concentration

Immuno-reactivity occurred owing to BBB disruption and immune cell infiltration in PTZ-induced epileptic seizures (figure 5B). As a result, significantly ($p < 0.001$) higher concentrations of anti-MOG antibodies were formed in mice with PTZ-induced epileptic seizures than in the vehicle control group. However, Puerarin (100 g $kg^{-1}$) remarkably reduced ($p < 0.001$) the immuno-reactivity and formation of anti-MOG antibodies.

## 3.6. Effect on reduced scattering coefficient owing to demyelination

Reduced scattering coefficient ($\mu_s$) is the optical parameter that changes owing to demyelination and differentiates the demyelinated samples [15]. Following the investigational procedure and data acquisition protocols, $\mu_s$ values of the mice brains were plotted using Origin software. The data were processed for the whole range of wavelengths. Figure 6 indicates that the $\mu_s$ trend follows the scattering-phase theorem [58]. For all the samples, $\mu_s$ was proportional to the phase variance, i.e. a decrease in $\mu_s$ with the increase of wavelength. Moreover, a huge difference in $\mu_s$ is found among the three groups, as shown in figure 6. It is evident from the results that the mice brains from the PTZ-induced epileptic seizures group showed the highest $\mu_s$ value compared with the other two groups of animals. The $\mu_s$ range of the PTZ-induced epileptic seizures group was 1.93982–1.33593 $cm^{-1}$. The brain samples of the Puerarin-treated group showed a reduction in the overall $\mu_s$ value. For the Puerarin-treated mouse brain, the $\mu_s$ range was 1.91859–1.21509 $cm^{-1}$. The result is closer to the $\mu_s$ value of the vehicle control group of animals, which ranges from 1.87289 to 1.14691 $cm^{-1}$.

## 3.7. Effect on molar absorption coefficient owing to demyelination

Molar absorption coefficient ($\mu_a$) is the optical parameter that reduces with the increase in demyelination owing to a reduction in neuron density [59]. The vehicle control group showed overall highest $\mu_a$ values (ranging from 1.26540 to 0.00404 $cm^{-1}$).

Downloaded from royalsocietypublishing.org/rsif/article-pdf/doi/10.1098/rsif.2025.0990/6127383/rsif.2025.0990.pdf
by guest
on 22 September 2026

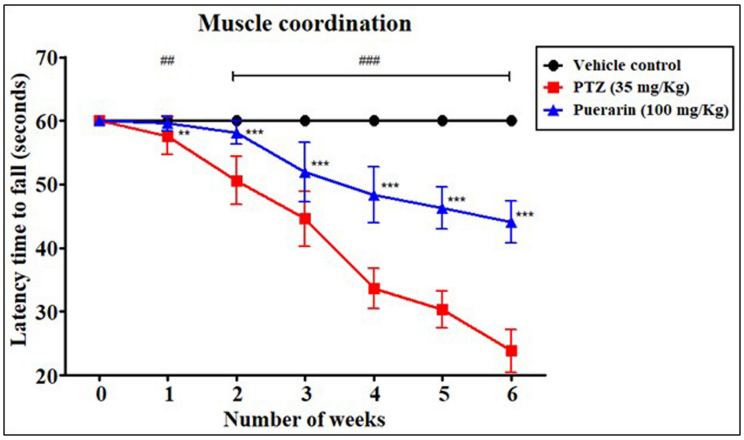



**Figure 3.** Puerarin exhibited progress in muscle coordination by improving latency time to fall owing to PTZ-induced epileptic seizures. Latency time to fall in seconds is indicated in mean ± s.d. for 12 mice in each group ($n = 12$). Significance level ** $p < 0.01$ and *** $p < 0.001$ represent the comparison of Puerarin effect with PTZ-administered group mice; however, ## $p < 0.01$ and ### $p < 0.001$ show comparison between PTZ-induced epileptic seizures group and vehicle control group of animals.

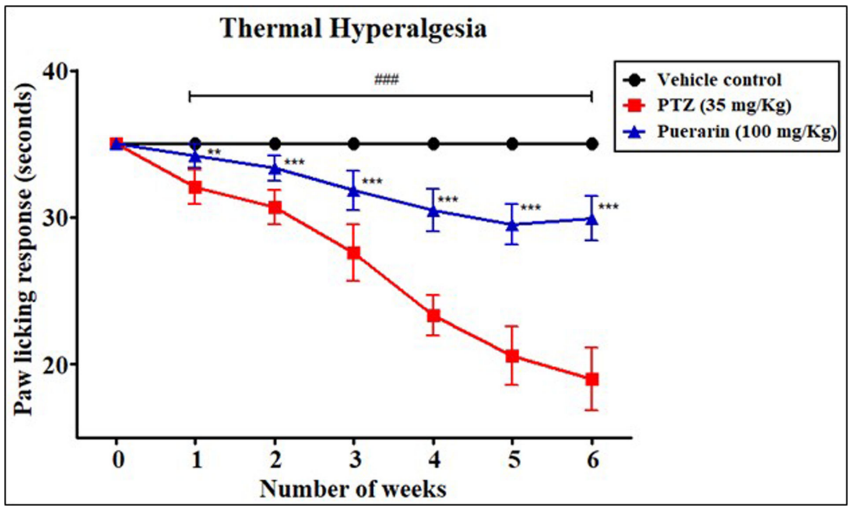



**Figure 4.** Puerarin showed a reduction in thermal hyperalgesia owing to PTZ-induced epileptic seizures by improving paw licking response time in seconds. Paw licking response is indicated in mean ± s.d. for 12 mice in each group ($n = 12$). Significance level ** $p < 0.01$ and *** $p < 0.001$ represent the comparison of Puerarin protective potential with PTZ-administered group mice; however, ### $p < 0.001$ shows comparison between PTZ-induced epileptic seizure group and vehicle control group of animals.

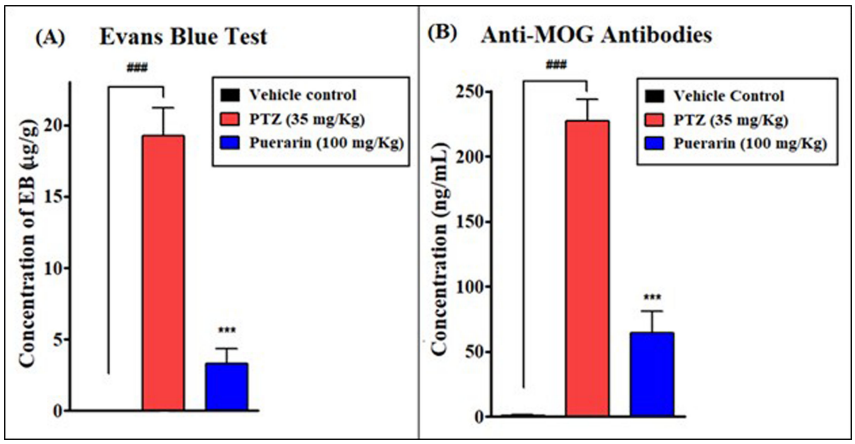



**Figure 5.** Puerarin considerably controlled the disruption of the blood-brain barrier and immune reactivity owing to PTZ-induced epileptic seizures by reducing the concentration of Evans blue dye (A) and anti-MOG antibodies (B). Mean ± s.d. ($n = 3$) for each group is presented in the results. Significance level *** $p < 0.001$ exhibits comparison of Puerarin protective effect with PTZ-administered group mice; however, ### $p < 0.001$ shows comparison between PTZ-induced epileptic seizure group and vehicle control group of animals.

PTZ-induced epileptic seizures cause a reduction in overall $\mu_a$ values (0.10957 $cm^{-1}$–0.00090542 $cm^{-1}$). However, $\mu_a$ values prominently improved in Puerarin-pretreated animals, ranging from 0.14624 to 0.00164 $cm^{-1}$ (figure 7).

Downloaded from royalsocietypublishing.org/rsif/article-pdf/doi/10.1098/rsif.2025.0990/6127383/rsif.2025.0990.pdf
by guest
on 22 September 2026

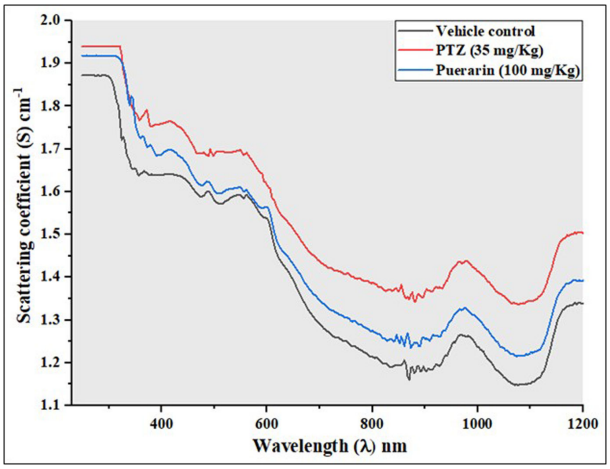



**Figure 6.** Puerarin's effect on the scattering coefficient ($\mu_s$) caused owing to demyelination in PTZ-induced epileptic seizures. Puerarin prominently reduced $\mu_s$ in mice compared with PTZ-induced epileptic seizures. Values of $\mu_s$ are plotted against increase in the wavelength (λ). The results exhibit the trend of scattering-phase theorem.

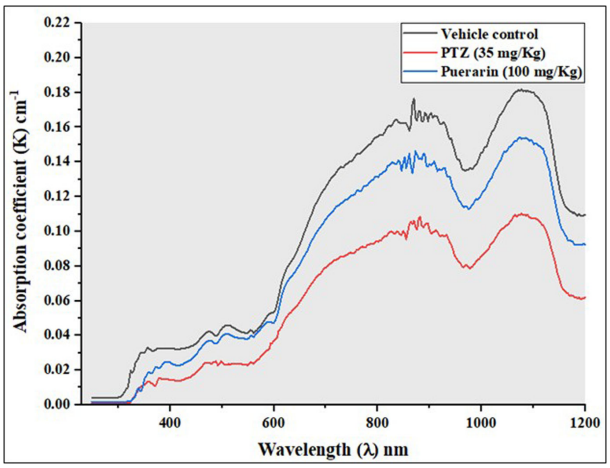



**Figure 7.** Puerarin's effect on absorption coefficient ($\mu_a$) is caused owing to demyelination and reduced cell density in PTZ-induced epileptic seizures. Puerarin prominently enhanced $\mu_a$ in the mice compared with PTZ-induced epileptic seizures. Values of $\mu_a$ are plotted against the increase of the wavelength (λ).

## 3.8. Effect on UV-vis diffuse reflectance spectroscopy absorption spectra of the brain

Absorption spectra of the normal and Puerarin-treated brains was profoundly different from the brain with epileptic seizures [60]. Figure 8 indicates the absorption spectra of the brain samples from all groups. Brain samples of the vehicle control group and Puerarin-treated animals showed high absorption for the complete range of wavelengths. However, the PTZ-treated group showed lower absorption. All the groups showed higher absorption from 250 to 600 nm wavelength that gradually decreased with the increase of wavelength.

## 3.9. Effect on band gap energy shift among the groups

The band gap energy ($E_{bg}$) shift was observed by comparing the results of three groups. $E_{bg}$ of the vehicle control group was lowest among all, i.e. 1.064 eV. Brain samples of PTZ-induced epileptic mice showed an increase in $E_{bg}$, which was 1.097 eV. However, the animals from the Puerarin pretreated group exhibited $E_{bg}$ of 1.065 eV, which was closer to the vehicle control group. Among the three groups, a blue shift of $E_{bg}$ was detected. The graphical plot is presented in figure 9.

## 3.10. Effect on nerve electrical conductivity of brain samples

Results of $E_{bg}$ were used for the approximation of nerve electrical conductivity ($\sigma$) of brain samples. The $\sigma$ of the vehicle control group was highest among the three groups, i.e. 0.943396226. Contrary to this, PTZ-induced epileptic seizures reduced $\sigma$ with a value of 0.911577028 owing to disrupted myelin sheath. Compared with this, Puerarin (100 mg $kg^{-1}$) treatment maintained the value of $\sigma$ as 0.938967136. Table 1 presents the values of $\sigma$ along with their $E_{bg}$ values to show a comparison.

Downloaded from royalsocietypublishing.org/rsif/article-pdf/doi/10.1098/rsif.2025.0990/6127383/rsif.2025.0990.pdf
by guest
on 22 September 2026

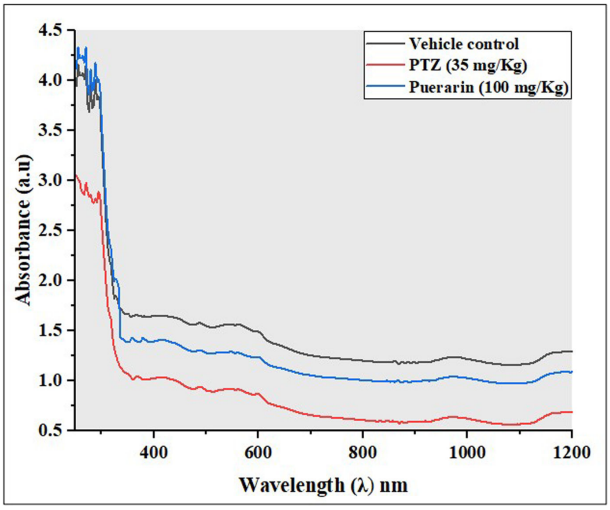



**Figure 8.** Puerarin's effect on absorption (A) is caused owing to myelin loss in PTZ-induced epileptic seizures. Puerarin prominently enhanced A in the mice compared with PTZ-induced epileptic seizures. Values of 'A' are plotted against the increase of the wavelength (λ).

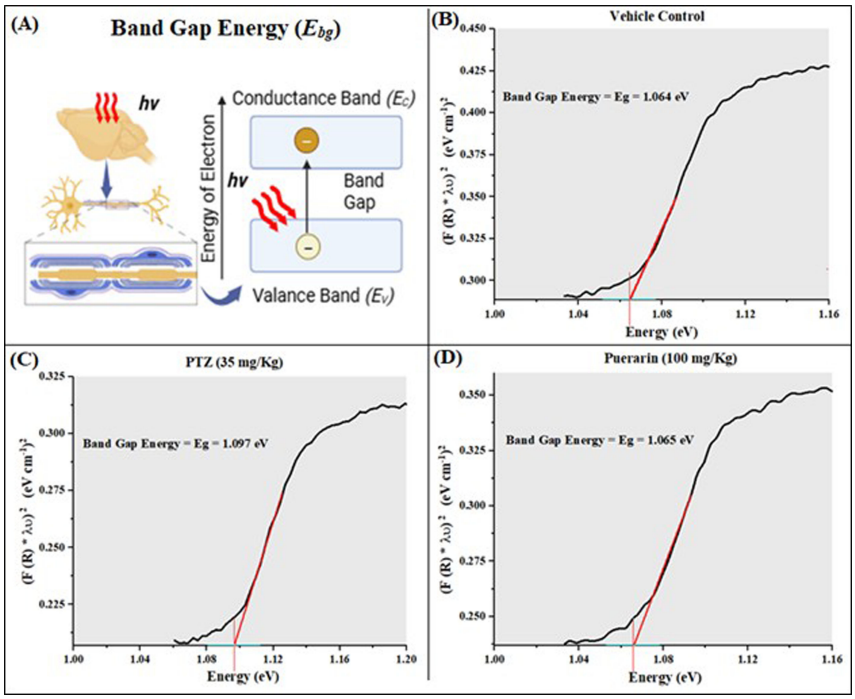



**Figure 9.** Puerarin effect on band gap energy ($E_{bg}$) shift triggered owing to demyelination of CNS nerves in PTZ-induced epileptic seizures. Illustration of demyelination and $E_{bg}$ concept (A). Overall, $E_{bg}$ exhibits a blue shift owing to demyelination as $E_{bg}$ values are shown in the vehicle control group (B), PTZ-induced epileptic mice (C), and Puerarin pretreated mice (D). The Kubelka–Munk model was used for approximation of $E_{bg}$, and $F(R_\infty)*hv^{1/2}$ was plotted against energy (eV).

## 3.11. Effect on the histopathological factor in haematoxylin and eosin staining

H&E staining results showed the normal neuron cells in the hippocampus and prefrontal cortex (PFC) of the vehicle control group (figure 10A–F). However, histopathological alteration ($p < 0.001$) in the brain cortex and hippocampus appeared in the PTZ-treated group compared with the vehicle control group. Demyelination owing to epileptic seizures causes nuclear shrinkage, loss of neurons and a higher level of vacuolation in the brain sections taken from the PTZ-treated mice. However, Puerarin treatment significantly ($p < 0.001$) alleviated this histopathological alteration.

## 3.12. The effect on neuronal density owing to epileptic seizures led to demyelination

Nissl staining showed intact cells and cell density with intense staining of Nissl bodies and DNA staining of nerve nucleus in the hippocampus and PFC of the vehicle control group (figure 10G–L). Contrary to this, the brain sections taken from PTZ-treated mice had more significant ($p < 0.001$) nerve damage and lower cell density than the vehicle control. In comparison, Puerarin treatment significantly ($p < 0.001$) countered the reduction of cell density caused by demyelination owing to epileptic seizures.

Downloaded from royalsocietypublishing.org/rsif/article-pdf/doi/10.1098/rsif.2025.0990/6127383/rsif.2025.0990.pdf
by guest
on 22 September 2026

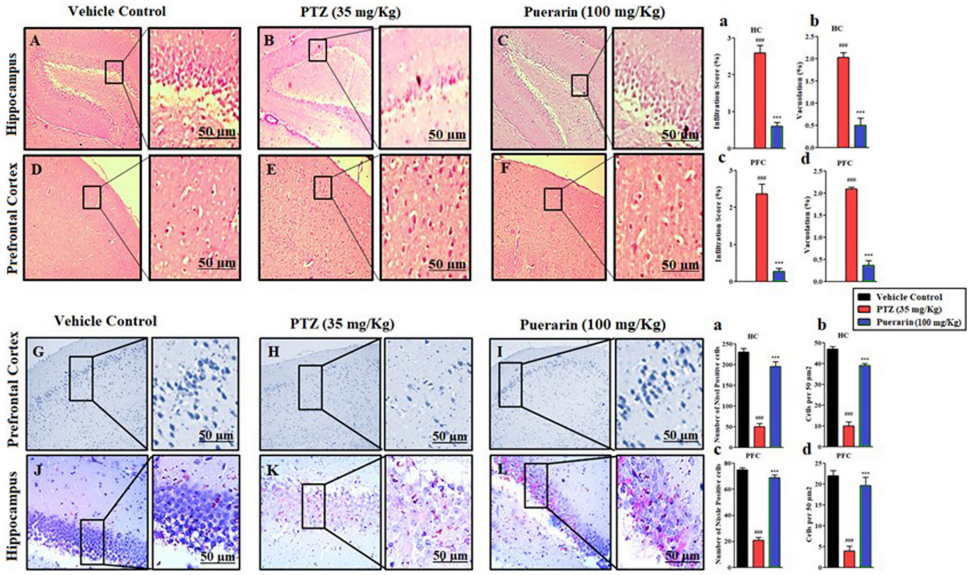



**Figure 10.** Puerarin treatment reduced histopathological changes in the hippocampus, scale bar = 50 µm, (A) vehicle control, (B) PTZ control, and (C) Puerarin. (a) and (b) Quantification in hippocampus histopathology. Pre-frontal cortex, scale bar = 50 µm, (E) vehicle control, (F) PTZ control and (G) Puerarin. (c) and (d) Quantification of pre-frontal cortex histopathology. Pre-frontal cortex stained with Nissl stain, scale bar = 50 µm, (G) vehicle control, (H) PTZ control and (I) Puerarin. (a) and (b) Quantification of pre-frontal cortex histopathology. Hippocampus, scale bar = 50 µm, (J) vehicle control, (K) PTZ control and (L) Puerarin. (c) and (d) Quantification of pre-frontal cortex histopathology. Results are presented as mean ± s.d. ($n = 3$), where *** $p < 0.001$ represents significance as compared with epileptic mice (PTZ 35 mg kg$^{-1}$). ### $p < 0.001$ represents significance as compared with vehicle control.

**Table 1.** Correlation between band gap energy and electrical conductivity of the brain samples taken from different groups.

| Sr. no. | experimental groups | band gap energy (eV) | electrical conductivity ($\sigma$) |
|---|---|---|---|
| 1. | vehicle control | 1.064 | 0.943396226 |
| 2. | PTZ (35 mg kg$^{-1}$) | 1.097 | 0.911577028 |
| 3. | Puerarin (100 mg kg$^{-1}$) | 1.065 | 0.938967136 |

## 4. Discussion

In the current experimental study, the neuroprotective effect of Puerarin was investigated against the demyelination and low $\sigma$ of CNS nerves in epileptic seizures. A novel and less invasive method (DRS) was adopted to assess these factors, i.e. band gap energy shift. Further, mathematical simulation using Kubelka–Munk theory was adopted in combination with common *in vivo* and *in vitro* laboratory techniques to cross-check the DRS results. Epileptic seizures and subsequent demyelination were induced using PTZ (35 mg kg$^{-1}$) i.p. injection on alternate days for six weeks. Seizure scoring exhibited a significant Puerarin (100 mg kg$^{-1}$) protective effect during 30 min of observation. Moreover, behavioural assessment is performed for the detection of demyelination and reduced $\sigma$ at the end of every week. PTZ-induced epileptic seizures prominently reduced muscle coordination and invoked thermal hyperalgesia [61]. Therefore, these behavioural factors are the close expression of demyelination in CNS nerves. These outcomes were further strengthened by the reported studies [6,33,61]. The results exhibited significant improvement in motor coordination owing to Puerarin pretreatment compared with the mice with epileptic seizures. Additionally, Puerarin showed more prominent protection against thermal hyperalgesia than the PTZ-treated animals. The behavioural assessment demonstrated Puerarin's protective effect against demyelination and low $\sigma$ caused by epileptic seizures in mice.

Structurally compromised BBB and immuno-reactivity are common mechanisms for the pathogenesis of demyelination of the CNS in epileptic seizures [62,63]. Neuronal hyper-excitation in epileptic seizures causes activation of the innate immune system, and subsequently, it makes the BBB structurally compromised [64]. BBB disruption causes infiltration of more immune cells [40]. Resultantly, anti-MOG antibodies are formed in epilepsy. These antibodies are considered an indicator factor for demyelination [39]. MOG is important for the myelination of nerves as well as for immune responses in the CNS [65]. Therefore, in the current study, EB dye infiltration and anti-MOG antibodies were checked in all samples to verify the induction of demyelination. Results indicated prominent BBB disruption and higher concentration of anti-MOG antibodies in PTZ-treated mice than in the vehicle control group. Puerarin (100 mg kg$^{-1}$) significantly protected the structural integrity of the BBB. Moreover, Puerarin protected against immuno-reactivity and subsequently the formation of antibodies against MOG. The results further strengthen the hypothesis that Puerarin has neuroprotective potential against demyelination owing to epileptic seizures.

After authenticating the induction, spectroscopic analysis was performed to evaluate Puerarin effect on demyelination and nerve $\sigma$ in epileptic seizures. Intrinsic optical properties of brain samples were determined through DRS. It was adopted

Downloaded from royalsocietypublishing.org/rsif/article-pdf/doi/10.1098/rsif.2025.0990/6127383/rsif.2025.0990.pdf
by guest
on 22 September 2026

based on the less invasive and more attractive technique for researchers. Furthermore, Kubelka–Munk theory was adopted for simulation, considering the heterogeneity and infinity of samples [66]. The Kubelka–Munk model is already the centre of attraction for scientists, particularly for the assessment of neuropathologies and disease prognosis [67]. After scanning the brain samples, $\mu_s$ was measured by adopting the established protocols. Change in $\mu_s$ is well reported, indicating optical property for demyelination of nerves in CNS and spinal cord [68]. Reported factors are myelin content, neuronal cell bodies and roughness of the nerves that affect $\mu_s$. It was observed in the results that the trend of $\mu_s$ versus wavelength followed the scattering-phase theorem. The reported theorem manifested as the overall increase in $\mu_s$ with the increase of tissue roughness. The inflamed and disrupted nerve cells enhance the tissue roughness, and resultantly, $\mu_s$ increases [69]. The same $\mu_s$ increase manifested in our results for mice with epileptic seizures as in Puerarin-treated mice. Moreover, the reported data revealed that the myelin sheath thinning causes a decrease in $\mu_s$ compared with highly myelinated nerves. However, our results indicated a prominent increase in $\mu_s$ for mice with epileptic seizures compared with vehicle control [15,68]. Wang *et al.* [58] coined a concept of phase gradient of tissue. The propagated light ray faces a tilt or change in direction or angle [58]. This can be a possible reason that the fragmented myelin content and intrusion of peripheral immune cells act as internal light scatterers in samples from epileptic seizure mice. The higher number of light scatterers offers more phases to change the propagated light path, and hence, the $\mu_s$ increases in brain samples with epileptic seizures. DePaoli *et al*. in 2020 also reported the same angle-based propagation of light and its effect on $\mu_s$ [68]. Contrary to this, Puerarin remarkably maintained the structural integrity of myelin sheath and nerves; therefore, it showed $\mu_s$ reduction of brain tissues; and hence, it protected against demyelination.

In addition to this, the results of $\mu_a$ further support the hypothesis of the neuroprotective effect of Puerarin against demyelination in epileptic seizures. Results clearly demonstrated a reduction in $\mu_a$ of the mice's brains having PTZ-induced epileptic seizures. However, samples from the vehicle control and the Puerarin pretreated group of animals showed higher $\mu_a$. Reported studies are also strengthening the hypothesis with the current results. Zou *et al*. in 2017 propagated the concept of a linear increase of $\mu_a$ with the increase in myelin content of the samples [70]. The possible mechanism behind this optical characteristic is enhanced lipid density. The highly myelinated brain area contains high lipid density owing to the lipid nature of the myelin sheath. Moreover, the synthesis of myelin sheath requires fatty acids that undergo lipid synthesis and form the main components of the myelin sheath [71]. The main constituents are lecithin and cholesterol. Therefore, the brain samples with high lipid concentration show higher $\mu_a$ and hence have high myelin content [70]. Moreover, the high density of neurons in normal brains exhibits higher $\mu_a$ than the brain samples of epileptic mice. The study reported by Zhu *et al.* further supports the current results regarding neuron density [59]. Contrary to this, PTZ-induced epileptic seizure reduces the neuronal density owing to hyper-excitability and cell death [72]. Our current results also support this finding by demonstrating reduced $\mu_a$ levels in mice experiencing PTZ-induced epileptic seizures.

In comparison with the $\mu_a$, the optical absorbance of the tissue provides indication of the overall absorbance of the photons by the samples. The measurement of the absorbance of biological tissue is not preferred owing to the scattering effect. The biological samples, in this case brain samples, have a large number of components that cause strong scattering of the absorbed light [73]. Consequently, the term absorbance is also referred to as the optical density. The scattering effect in the overall absorbance causes deviation of the measured light at different angles from the direct path. Hence, in order to ignore the effect of scattering molecules in the brain tissue and to assess the effect on the basis of true absorbance, molar absorption coefficient was measured [74]. The figure 7 of the molar absorption coefficient and figure 8 of optical absorbance spectra clearly indicate the difference that is caused by scattering effect. In figure 8, a high absorption coefficient is indicated in the end of the visible red light spectrum and near-infrared (IR) region that lies under 600–1200 nm wavelength. It is a well-reported fact that high penetration of the light is observed at this wavelength [75]. Therefore, the light absorbers or chromophores deep into the tissue, such as water and haemoglobin, show significant absorbance at this range [76]. The reported data further support the results indicated in figures 7 and 8. However, the general effect of demyelination can be assessed with the overall absorbance spectra. Demyelination involves loss of myelin and hence the demyelinated samples show less absorbance compared with normal samples [60,70].

By simulating with the Kubelka–Munk model, $E_{bg}$ was calculated separately for samples of each group. $E_{bg}$ is the intrinsic ability of the matter to conduct electrical signals [77]. $E_{bg}$ is the energy required for the movement of an electron from the valence band to the conduction band. If the matter is a good conductor, it will have less $E_{bg}$. The conduction of an impulse through electron movement will be easy. Contrary to this, a reduction in conduction ability will show a high $E_{bg}$ value. Similarly, in biological tissues, an action potential is generated owing to ion movement across the cell membrane and generates electrical impulses. In the CNS, the action potential is stronger owing to the involvement of synapse. Therefore, the optical characteristic is a closer indicator of the conduction ability of brain samples. Additionally, the excitation of electrons via photon propagation is a well-documented phenomenon, and our results support this hypothesis [78]. Therefore, the epileptic brain showed higher $E_{bg}$ value owing to demyelination and reduced ability to generate impulse than vehicle and Puerarin-treated group. In addition to this, the $E_{bg}$ shift was observed as a blue shift among the groups. Blue shift is referred to as an increase in $E_{bg}$ value. The vehicle control group showed the lowest $E_{bg}$ value. Puerarin-pretreated mice showed slightly higher $E_{bg}$ values. However, the PTZ-treated mice exhibited the highest $E_{bg}$ value, as shown in table 1. The blue shift strongly corresponds with reduced conductivity of matter [79]. Therefore, it further authenticates the previous findings that Puerarin protects against demyelination.

Histopathological analysis was performed to further authenticate the results of spectroscopic assessment. H&E staining was conducted to verify whether the normal neuron density was altered owing to PTZ-induced epileptic seizures. The results explicated that Puerarin significantly maintained the normal tissue structure of the brain hippocampus and cerebral cortex compared with the negative control group. Additionally, Nissl staining was executed to find the neuron density in the samples of all groups. The lowest neuron density was found in PTZ-induced epileptic seizure mice. In contrast, Puerarin significantly

Downloaded from royalsocietypublishing.org/rsif/article-pdf/doi/10.1098/rsif.2025.0990/6127383/rsif.2025.0990.pdf
by guest
on 22 September 2026

preserved the neurons and maintained the density of normal neurons in both the cerebral cortex and the hippocampus. These results further support the DRS results and band gap energy concept in biological tissue samples. In short, PTZ-induced epileptic seizures cause demyelination owing to the formation of anti-MOG antibodies and BBB disruption. Immune reactivity and cascade of demyelination led to a reduction in cell density, and hence, reduction in $\sigma$ of samples. However, Puerarin exhibited protective influence against demyelination and low $\sigma$ by maintaining the normal tissue structure and neuronal cell density. Results are in correlation with the $\mu_a$, $\mu_s$ and $E_{bg}$ corresponding to the intrinsic $\sigma$ of samples.

## 5. Conclusion

In conclusion, the study demonstrates that Puerarin provides significant neuroprotection against demyelination and reduced intrinsic sigma activity associated with PTZ-induced epileptic seizures. Puerarin significantly countered epileptic seizures and their associated BBB disruption. The resultant immuno-reactivity was reduced by inhibiting the formation of antibodies against the MOG protein. The effect, subsequently, preserved the myelin sheath and basic tissue morphology. In spectroscopic analysis, Puerarin showed similar results by enhancing $\mu_a$, reducing $\mu_s$ and $E_{bg}$ shift, and consequently, the intrinsic ability of brain samples to conduct impulses after stimulation and excitation of electrons with photonic energy. Histopathological assessment further supports the results. However, keeping in view the introduction of band gap energy shift in biological samples, there is a need for a more detailed study with different simulation models to further improve the literature on brain optical properties.

Ethics. The study was held after attaining ethical approval (BEC-FBS-QAU2022-422) of the Bioethical Committee, Quaid-i-Azam University, Islamabad and compliance was ensured as per guidelines.

Data accessibility. Data are available in the article's supplementary material. The data supporting (RAW data) the current research work are provided as supplementary files.

Supplementary material is available online [80].

Declaration of AI use. We have not used AI-assisted technologies in creating this article.

Authors' contributions. S.B.: conceptualization, data curation, formal analysis, investigation, methodology, software, validation, visualization, writing—original draft; T.B.: investigation, methodology, visualization, writing—review and editing; M.I.K.: investigation, methodology, software, writing—review and editing; K.U.S.: methodology, software, writing—review and editing; F.U.: investigation, methodology; H.A.: methodology, writing—review and editing; A.S.: methodology, writing—review and editing; E.K.S.: validation, writing—review and editing; S.K.: conceptualization, data curation, formal analysis, investigation, methodology, software, supervision, validation, visualization, writing—review and editing.

All authors gave final approval for publication and agreed to be held accountable for the work performed therein.

Conflict of interest declaration. We declare we have no competing interests.

Funding. The Higher Education Commission provided funding for the project under the Indigenous Fellowship Program vide letter no. 520(Ph-II)/2MD6-046/HEC/IS/2020.

## References

1. Manole AM, Sirbu CA, Mititelu MR, Vasiliu O, Lorusso L, Sirbu OM, Ionita Radu F. 2023 State of the art and challenges in epilepsy—a narrative review. *J. Pers. Med*. **13**, 623. (doi:10.3390/jpm13040623)
2. Cao Y *et al*. 2022 Dysfunction of the hippocampal-lateral septal circuit impairs risk assessment in epileptic mice. *Front. Mol. Neurosci*. **15**, 828891. (doi:10.3389/fnmol.2022.828891)
3. Avoli M, Louvel J, Pumain R, Köhling R. 2005 Cellular and molecular mechanisms of epilepsy in the human brain. *Prog. Neurobiol*. **77**, 166–200. (doi:10.1016/j.pneurobio.2005.09.006)
4. Sun ZQ, Meng FH, Tu LX, Sun L. 2019 Myricetin attenuates the severity of seizures and neuroapoptosis in pentylenetetrazole kindled mice by regulating the of BDNF-TrkB signaling pathway and modulating matrix metalloproteinase-9 and GABAA. *Exp. Ther. Med*. **17**, 3083–3091. (doi:10.3892/etm.2019.7282)
5. Fabene PF *et al*. 2008 A role for leukocyte-endothelial adhesion mechanisms in epilepsy. *Nat. Med*. **14**, 1377–1383. (doi:10.1038/nm.1878)
6. You Y, Bai H, Wang C, Chen LW, Liu B, Zhang H, Gao GD. 2011 Myelin damage of hippocampus and cerebral cortex in rat pentylenetetrazol model. *Brain Res*. **1381**, 208–216. (doi:10.1016/j.brainres.2011.01.011)
7. Pirko I, Noseworthy JH. 2009 Demyelinating disorders of the central nervous system. In *Textbook of clinical neurology* (eds I Pirko, JH Noseworthy), pp. 1103–1133, 3rd edn. Boca Raton, FL: Elsevier. (doi:10.1016/B978-141603618-0.10048-7)
8. Eliseeva DD, Zakharova MN. 2023 Myelin oligodendrocyte glycoprotein as an autoantigen in inflammatory demyelinating diseases of the central nervous system. *Biochem. Biokhimiia* **88**, 551–563. (doi:10.1134/S0006297923040107)
9. Calabrese M *et al*. 2008 Extensive cortical inflammation is associated with epilepsy in multiple sclerosis. *J. Neurol*. **255**, 581–586. (doi:10.1007/s00415-008-0752-7)
10. Perucca E *et al*. 2024 Which terms should be used to describe medications used in the treatment of seizure disorders? An ILAE position paper. *Epilepsia* **65**, 533–541. (doi:10.1111/epi.17877)
11. Shoeibi A *et al*. 2021 Epileptic seizures detection using deep learning techniques: a review. *Int. J. Environ. Res. Public Health* **18**, 5780. (doi:10.3390/ijerph18115780)
12. Prayson RA. 2010 Diagnostic challenges in the evaluation of chronic epilepsy-related surgical neuropathology. *Am. J. Surg. Pathol*. **34**, e1–e13. (doi:10.1097/PAS.0b013e3181d9ba38)
13. Zienowicz M, Wisłowska A, Lehner M, Taracha E, Skórzewska A, Maciejak P, Płaźnik A. 2005 The effect of fluoxetine in a model of chemically induced seizures—behavioral and immunocytochemical study. *Neurosci. Lett*. **373**, 226–231. (doi:10.1016/j.neulet.2004.10.009)
14. Eggert HR, Blazek V. 1987 Optical properties of human brain tissue, meninges, and brain tumors in the spectral range of 200 to 900 nm. *Neurosurgery* **21**, 459–464. (doi:10.1227/00006123-198710000-00003)

Downloaded from royalsocietypublishing.org/rsif/article-pdf/doi/10.1098/rsif.2025.0990/6127383/rsif.2025.0990.pdf
by guest
on 22 September 2026

15. Radhakrishnan H, Senapati A, Kashyap D, Peng YB, Liu H. 2005 Light scattering from rat nervous system measured intraoperatively by near-infrared reflectance spectroscopy. *J. Biomed. Opt*. **10**, 051405. (doi:10.1117/1.2098487)
16. Tri PN, Rtimi S, Nguyen TA, Vu MT. 2019 Chapter 5 – Physics, electrochemistry, photochemistry, and photoelectrochemistry of hybrid nanoparticles. In *Noble metal-metal oxide hybrid nanoparticles* (eds S Mohapatra, TA Nguyen, P Nguyen-Tri), pp. 95–123. Cambridge, UK: Woodhead Publishing. (doi:10.1016/B978-0-12-814134-2.00005-X)
17. Makuła P, Pacia M, Macyk W. 2018 How to correctly determine the band gap energy of modified semiconductor photocatalysts based on UV–vis spectra. *J. Phys. Chem. Lett*. **9**, 6814–6817. (doi:10.1021/acs.jpclett.8b02892)
18. Khan A, Tayara H, Chong KT. 2023 Prediction of organic material band gaps using graph attention network. *Comput. Mater. Sci*. **220**, 112063. (doi:10.1016/j.commatsci.2023.112063)
19. Wang F, He M, Huang B, Tang T, Liu F, Cui R, Qian J, Zhang M, Sun T. 2023 Band gap engineering improves three-photon luminescence of quantum dots for deep brain imaging. *Anal. Chem*. **95**, 10947–10956. (doi:10.1021/acs.analchem.3c00845)
20. Chaachouay N, Zidane L. 2024 Plant-derived natural products: a source for drug discovery and development. *Drugs Drug Candidates* **3**, 184–207. (doi:10.3390/ddc3010011)
21. Bacanlı M, Aydın S, Başaran AA, Başaran N. 2018 Chapter 33 – A phytoestrogen puerarin and its health effects. In *Polyphenols: prevention and treatment of human disease* (eds RR Watson, VR Preedy, S Zibadi), pp. 425–431, 2nd edn. Cambridge, MA, USA: Academic Press. (doi:10.1016/B978-0-12-813008-7.00033-3)
22. Yuan M, He Q, Xiang W, Deng Y, Lin S, Zhang R. 2024 Natural compounds efficacy in ophthalmic diseases: a new twist impacting ferroptosis. *Biomed. Pharmacother.* **172**, 116230. (doi:10.1016/j.biopha.2024.116230)
23. Wang Q, Li W, Hu H, Lu X, Qin S. 2023 Monomeric compounds from traditional Chinese medicine: new hopes for drug discovery in pulmonary fibrosis. *Biomed. Pharmacother*. **159**, 114226. (doi:10.1016/j.biopha.2023.114226)
24. Bina F, Soleymani S, Toliat T, Hajimahmoodi M, Tabarrai M, Abdollahi M, Rahimi R. 2019 Plant-derived medicines for treatment of endometriosis: a comprehensive review of molecular mechanisms. *Pharmacol. Res*. **139**, 76–90. (doi:10.1016/j.phrs.2018.11.008)
25. Shao H, Huang Y, Xu D, Huang S, Tong R. 2022 A systematic review and meta-analysis on the efficacy of puerarin injection as adjunctive therapy for unstable angina pectoris. *Front. Cardiovasc. Med.* **9**, 763567. (doi:10.3389/fcvm.2022.763567)
26. Kazmi Z, Zeeshan S, Khan A, Malik S, Shehzad A, Seo EK, Khan S. 2020 Anti-epileptic activity of daidzin in PTZ-induced mice model by targeting oxidative stress and BDNF/VEGF signaling. *Neurotoxicology* **79**, 150–163. (doi:10.1016/j.neuro.2020.05.005)
27. Tawfik KM, Moustafa YM, El-Azab MF. 2018 Neuroprotective mechanisms of sildenafil and selenium in PTZ-kindling model: implications in epilepsy. *Eur. J. Pharmacol*. **833**, 131–144. (doi:10.1016/j.ejphar.2018.05.035)
28. Racine RJ. 1972 Modification of seizure activity by electrical stimulation. II. Motor seizure. *Electroencephalogr. Clin. Neurophysiol*. **32**, 281–294. (doi:10.1016/0013-4694(72)90177-0)
29. Kajita Y, Mushiake H. 2024 Dynamic changes in seizure state and anxiety-like behaviors during pentylenetetrazole kindling in rats. *Epilepsy Behav*. **159**, 110019. (doi:10.1016/j.yebeh.2024.110019)
30. Kamil K, Yazid MD, Idrus RBH, Das S, Kumar J. 2019 Peripheral demyelinating diseases: from biology to translational medicine. *Front. Neurol*. **10**, 87. (doi:10.3389/fneur.2019.00087)
31. Deacon RM. 2013 Measuring the strength of mice. *J. Vis. Exp.* **76**, e2610. (doi:10.3791/2610)
32. Shal B, Khan A, Naveed M, Ali H, Seo EK, Choi H, Khan S. 2020 Neuroprotective effect of 25-methoxyhispidol a against CCl4-induced behavioral alterations by targeting VEGF/BDNF and caspase-3 in mice. *Life Sci*. **253**, 117684. (doi:10.1016/j.lfs.2020.117684)
33. Schuler V *et al*. 2001 Epilepsy, hyperalgesia, impaired memory, and loss of pre- and postsynaptic $GABA_B$ responses in mice lacking $GABA_{B(1)}$. *Neuron* **31**, 47–58. (doi:10.1016/s0896-6273(01)00345-2)
34. Marchi N *et al*. 2007 Seizure-promoting effect of blood–brain barrier disruption. *Epilepsia* **48**, 732–742. (doi:10.1111/j.1528-1167.2007.00988.x)
35. D'Aversa TG, Eugenin EA, Lopez L, Berman JW. 2013 Myelin basic protein induces inflammatory mediators from primary human endothelial cells and blood–brain barrier disruption: implications for the pathogenesis of multiple sclerosis. *Neuropathol. Appl. Neurobiol*. **39**, 270–283. (doi:10.1111/j.1365-2990.2012.01279.x)
36. Harford-Wright E, Lewis KM, Ghabriel MN, Vink R. 2014 Treatment with the NK1 antagonist emend reduces blood brain barrier dysfunction and edema formation in an experimental model of brain tumors. *PLoS One* **9**, e97002. (doi:10.1371/journal.pone.0097002)
37. Shal B *et al*. 2021 Alleviation of memory deficit by bergenin via the regulation of reelin and Nrf-2/NF-κB pathway in transgenic mouse model. *Int. J. Mol. Sci*. **22**, 6603. (doi:10.3390/ijms22126603)
38. Reindl M, Di Pauli F, Rostásy K, Berger T. 2013 The spectrum of MOG autoantibody-associated demyelinating diseases. *Nat. Rev. Neurol*. **9**, 455–461. (doi:10.1038/nrneurol.2013.118)
39. Foiadelli T, Gastaldi M, Scaranzin S, Franciotta D, Savasta S. 2020 Seizures and myelin oligodendrocyte glycoprotein (MOG) antibodies: two paradigmatic cases and a review of the literature. *Mult. Scler. Relat. Disord*. **41**, 102011. (doi:10.1016/j.msard.2020.102011)
40. Yamanaka G *et al*. 2021 Links between immune cells from the periphery and the brain in the pathogenesis of epilepsy: a narrative review. *Int. J. Mol. Sci*. **22**, 4395. (doi:10.3390/ijms22094395)
41. Haglund MM. 2012 Optical imaging of visual cortex epileptic foci and propagation pathways. *Epilepsia* **53**, 87–97. (doi:10.1111/j.1528-1167.2012.03479.x)
42. Yadav N, Bhatia S, Ragheb J, Mehta R, Jayakar P, Yong W, Lin WC. 2013 *In vivo* detection of epileptic brain tissue using static fluorescence and diffuse reflectance spectroscopy. *J. Biomed. Opt*. **18**, 027006. (doi:10.1117/1.jbo.18.2.027006)
43. Piper DJW, Pirmez C, Manley. PL, Long D, Flood RD, Normark WR, Showers W. 1997 Mass-transport deposits of the Amazon Fan. In *Proceedings of the ocean drilling program, scientific results*, pp. 109–146. College Station, TX, USA: Texas A & M University, Ocean Drilling Program. (doi:10.2973/odp.proc.sr.155.212.1997)
44. McNaught AD, Wilkinson A. 1997 *IUPAC, compendium of chemical terminology, the 'gold book'.* Oxford, UK: Blackwell Scientific Publications.
45. Volterrani M, Minelli A, Gaetani M, Grossi N, Magni S, Caturegli L. 2017 Reflectance, absorbance and transmittance spectra of bermudagrass and manilagrass turfgrass canopies. *PLoS One* **12**, e0188080. (doi:10.1371/journal.pone.0188080)
46. Blazek V. 1979 Absorption and scattering properties of biological tissue in relation to monochromatic optical radiation. *Biomed Tech*. **24**, 331–332.
47. Tao R, Gröhl J, Hacker L, Pifferi A, Roblyer D, Bohndiek SE. 2024 Tutorial on methods for estimation of optical absorption and scattering properties of tissue. *J. Biomed. Opt*. **29**, 060801. (doi:10.1117/1.jbo.29.6.060801)
48. Wei HJ, Xing D, Wu GY, Jin Y, Gu HM. 2003 Optical properties of human normal small intestine tissue determined by Kubelka-Munk method *in vitro*. *World J. Gastroenterol*. **9**, 2068–2072. (doi:10.3748/wjg.v9.i9.2068)
49. Militký J. 2011 3 - Fundamentals of soft models in textiles. In *Soft computing in textile engineering* (ed. A Majumdar), pp. 45–102. Cambridge, UK: Woodhead Publishing. (doi:10.1533/9780857090812.1.45)


Downloaded from royalsocietypublishing.org/rsif/article-pdf/doi/10.1098/rsif.2025.0990/6127383/rsif.2025.0990.pdf
by guest
on 22 September 2026

50. Sharma M, Yangui A, Whiteside VR, Sellers IR, Han D, Chen S, Du MH, Saparov B. 2019 $Rb_4Ag_2BiBr_9$: a lead-free visible light absorbing halide semiconductor with improved stability. *Inorg. Chem*. **58**, 4446–4455. (doi:10.1021/acs.inorgchem.8b03623)
51. Sawicki B, Tomaszewicz E, Piątkowska M, Groń T, Duda H, Górny K. 2016 Correlation between the band-gap energy and the electrical conductivity in $MPr_2W_2O_{10}$ tungstates (Where M = Cd, Co, Mn). *Acta Phys. Pol. A* **129**, A-94. (doi:10.12693/APhysPolA.129.A-94)
52. Bashir MBA, Mohd Said S, Sabri MFM, Shnawah DA, Elsheikh MH. 2014 Recent advances on $Mg_2Si_{1-x}Sn_x$ materials for thermoelectric generation. *Renew. Sustain. Energy Rev*. **37**, 569–584. (doi:10.1016/j.rser.2014.05.060)
53. Wu Q, Wang H. 2018 The spatiotemporal expression changes of CB2R in the hippocampus of rats following pilocarpine-induced status epilepticus. *Epilepsy Res*. **148**, 8–16. (doi:10.1016/j.eplepsyres.2018.10.002)
54. Gul M *et al*. 2022 Formulation optimization, *in vitro* and *in vivo* evaluation of agomelatine-loaded nanostructured lipid carriers for augmented antidepressant effects. *Colloids Surf. B. Biointerfaces* **216**, 112537. (doi:10.1016/j.colsurfb.2022.112537)
55. Yu X, Zhou T, Yu H, Chang LY, Wei LL. 2018 Corilagin reduces the frequency of seizures and improves cognitive function in a rat model of chronic epilepsy. *Med. Sci. Monit.* **24**, 2832–2840. (doi:10.12659/msm.906509)
56. Zhen J, Qu Z, Fang H, Fu L, Wu Y, Wang H, Zang H, Wang W. 2014 Effects of grape seed proanthocyanidin extract on pentylenetetrazole-induced kindling and associated cognitive impairment in rats. *Int. J. Mol. Med*. **34**, 391–398. (doi:10.3892/ijmm.2014.1796)
57. Wang Q, Shen ZN, Zhang SJ, Sun Y, Zheng FJ, Li YH. 2022 Protective effects and mechanism of puerarin targeting PI3K/Akt signal pathway on neurological diseases. *Front. Pharmacol*. **13**, 1022053. (doi:10.3389/fphar.2022.1022053)
58. Wang Z, Ding H, Popescu G. 2011 Scattering-phase theorem. *Opt. Lett*. **36**, 1215–1217. (doi:10.1364/OL.36.001215)
59. Zhu L, Zou Y, Li J, Liu Q. 2018 Terahertz spectroscopy of neurodegenerative diseases: the correlation between terahertz biophysics and pathological analysis. In *The 9th Int. Symp. on Ultrafast Phenomena and Terahertz Waves*. Changsha, Hunan: Optica Publishing Group. (doi:10.1364/ISUPTW.2018.TuF4)
60. Gakh O, Wilkins JM, Guo Y, Popescu BF, Weigand SD, Kalinowska-Lyszczarz A, Lucchinetti CF. 2024 Infrared spectral profiling of demyelinating activity in multiple sclerosis brain tissue. *Acta Neuropathol. Commun*. **12**, 146. (doi:10.1186/s40478-024-01854-4)
61. Naseer MI, Shupeng L, Kim MO. 2009 Maternal epileptic seizure induced by pentylenetetrazol: apoptotic neurodegeneration and decreased GABAB1 receptor expression in prenatal rat brain. *Mol. Brain* **2**, 20. (doi:10.1186/1756-6606-2-20)
62. Berghoff SA *et al*. 2017 Blood-brain barrier hyperpermeability precedes demyelination in the cuprizone model. *Acta Neuropathol. Commun*. **5**, 94. (doi:10.1186/s40478-017-0497-6)
63. Li J, Qi H, Chen Y, Zhu X. 2024 Epilepsy and demyelination: towards a bidirectional relationship. *Prog. Neurobiol*. **234**, 102588. (doi:10.1016/j.pneurobio.2024.102588)
64. Chen J, Yu H, Liu H, Yu H, Liang S, Wu Q, Zhang X, Zeng R, Diao L. 2024 Causal relationship between immune cells and epilepsy mediated by metabolites analyzed through Mendelian randomization. *Sci. Rep*. **14**, 19644. (doi:10.1038/s41598-024-70370-1)
65. Dale RC, Banwell B, Bar-Or A, Brilot F. 2012 Autoantibodies against aquaporin-4 and myelin oligodendrocyte glycoprotein in paediatric CNS demyelination: recent developments and future directions. *Mult. Scler. Relat. Disord*. **1**, 116–122. (doi:10.1016/j.msard.2012.03.003)
66. Li J, Xie D, Li M, Liu S, Wei CA. 2022 Optimal learning samples for two-constant Kubelka-Munk theory to match the color of pre-colored fiber blends. *Front. Neurosci.* **16**, 945454. (doi:10.3389/fnins.2022.945454)
67. Yona G, Meitav N, Kahn I, Shoham S. 2016 Realistic numerical and analytical modeling of light scattering in brain tissue for optogenetic applications(1,2,3). *eNeuro* **3**. (doi:10.1523/ENEURO.0059-15.2015)
68. DePaoli D *et al*. 2020 Anisotropic light scattering from myelinated axons in the spinal cord. *Neurophotonics* **7**, 015011. (doi:10.1117/1.NPh.7.1.015011)
69. Chang S *et al*. 2022 Scalable mapping of myelin and neuron density in the human brain with micrometer resolution. *Sci. Rep.* **12**, 363. (doi:10.1038/s41598-021-04093-y)
70. Zou Y *et al*. 2017 Terahertz spectroscopic diagnosis of myelin deficit brain in mice and rhesus monkey with chemometric techniques. *Sci. Rep*. **7**, 5176. (doi:10.1038/s41598-017-05554-z)
71. Poitelon Y, Kopec AM, Belin S. 2020 Myelin fat facts: an overview of lipids and fatty acid metabolism. *Cells* **9**, 812. (doi:10.3390/cells9040812)
72. Sumadewi KT, Harkitasari S, Tjandra DC. 2023 Biomolecular mechanisms of epileptic seizures and epilepsy: a review. *Acta Epileptol*. **5**, 28. (doi:10.1186/s42494-023-00137-0)
73. Cone MT *et al*. 2015 Measuring the absorption coefficient of biological materials using integrating cavity ring-down spectroscopy. *Optica* **2**, 162–168. (doi:10.1364/OPTICA.2.000162)
74. Hu C, Muller-Karger F, Zepp R. 2002 Absorbance, absorption coefficient, and apparent quantum yield: a comment on common ambiguity in the use of these optical concepts. *Limnol. Oceanogr.* **47**, 1261–1267. (doi:10.2307/3069048)
75. Bhattacharya M, Dutta A. 2019 Computational modeling of the photon transport, tissue heating, and cytochrome C oxidase absorption during transcranial near-infrared stimulation. *Biophysics* **9**, 179. (doi:10.1101/708362)
76. Hamdy O, Abdel-Salam Z, Abdel-Harith M. 2022 Optical characterization of biological tissues based on fluorescence, absorption, and scattering properties. *Diagnostics* **12**, 2846. (doi:10.3390/diagnostics12112846)
77. Nguyen-Tri P, Rtimi S, Nguyen TA, Vu M. 2019 Physics, electrochemistry, photochemistry, and photoelectrochemistry of hybrid nanoparticles. In *Polish archives of internal medicine* (eds S Mohapatra, TA Nguyen, NT Phuong), pp. 95–123. Cambridge, UK: Elsevier. (doi:10.1016/B978-0-12-814134-2.00005-X)
78. Iida K, Noda M. 2020 Electron transfer governed by light–matter interaction at metal–semiconductor interface. *Npj Comput. Mater*. **6**, 5. (doi:10.1038/s41524-019-0269-x)
79. You Q, Cai H, Hu Z, Liang P, Prucnal S, Zhou S, Sun J, Xu N, Wu J. 2015 Blue shift in absorption edge and widening of band gap of ZnO by Al doping and Al–N co-doping. *J. Alloy. Compd*. **644**, 528–533. (doi:10.1016/j.jallcom.2015.05.060)
80. Bano S, Bibi T, Khan MI, Shah KU, Ud-din F, Ali H *et al*. 2026 Supplementary material from: Band Gap Energy shift as a Biophysical Marker of Puerarin's Neuroprotective Role in Epilepsy-Induced Demyelination. Figshare (doi:10.6084/m9.figshare.c.8329018)


Downloaded from royalsocietypublishing.org/rsif/article-pdf/doi/10.1098/rsif.2025.0990/6127383/rsif.2025.0990.pdf
by guest
on 22 September 2026